ARMY RESEARCH LABORATORY

Low-Frequency Foam Insulator (LOFFI) Accelerometer Mount Characterization Results and Analysis for Phase I (FY2013)

by Andrew Drysdale, Ryan Sorensen, and Justin Pritchett

ARL-TR-6977 **June 2014**

NOTICES

Disclaimers

The findings in this report are not to be construed as an official Department of the Army position unless so designated by other authorized documents.

Citation of manufacturer's or trade names does not constitute an official endorsement or approval of the use thereof.

Destroy this report when it is no longer needed. Do not return it to the originator.

Army Research Laboratory
Aberdeen Proving Ground, MD 21005-5068

ARL-TR-6977 **June 2014**

Low-Frequency Foam Insulator (LOFFI) Accelerometer Mount Characterization Results and Analysis for Phase I (FY2013)

Andrew Drysdale, Ryan Sorensen, and Justin Pritchett
Survivability/Lethality Analysis Directorate, ARL

REPORT DOCUMENTATION PAGE			Form Approved OMB No. 0704-0188

1. REPORT DATE *(DD-MM-YYYY)*	2. REPORT TYPE	3. DATES COVERED (From - To)
June 2014	Final	January 2013–April 2014

4. TITLE AND SUBTITLE
Low-Frequency Foam Insulator (LOFFI) Accelerometer Mount Characterization Results and Analysis for Phase I (FY2013)

5a. CONTRACT NUMBER

5b. GRANT NUMBER

5c. PROGRAM ELEMENT NUMBER

6. AUTHOR(S)
Andrew Drysdale, Ryan Sorensen, and Justin Pritchett

5d. PROJECT NUMBER

5e. TASK NUMBER

5f. WORK UNIT NUMBER

7. PERFORMING ORGANIZATION NAME(S) AND ADDRESS(ES)
U.S. Army Research Laboratory
ATTN: RDRL-SLB-D
Aberdeen Proving Ground, MD 21005-5068

8. PERFORMING ORGANIZATION REPORT NUMBER
ARL-TR-6977

9. SPONSORING/MONITORING AGENCY NAME(S) AND ADDRESS(ES)

10. SPONSOR/MONITOR'S ACRONYM(S)

11. SPONSOR/MONITOR'S REPORT NUMBER(S)

12. DISTRIBUTION/AVAILABILITY STATEMENT
Approved for public release; distribution is unlimited.

13. SUPPLEMENTARY NOTES

14. ABSTRACT
The influence of the Low-Frequency Foam Insulator (LOFFI) accelerometer mount on measured data is characterized via the creation of a frequency-domain "gain" function from experimental data. This function is then applied to individual trials in order to determine the extent to which the gain function is able to replicate the LOFFI mount's influence.

15. SUBJECT TERMS
LOFFI, accelerometer, gain, frequency-response, low-frequency foam insulator

16. SECURITY CLASSIFICATION OF:			17. LIMITATION OF ABSTRACT	18. NUMBER OF PAGES	19a. NAME OF RESPONSIBLE PERSON
a. REPORT	b. ABSTRACT	c. THIS PAGE			Andrew Drysdale
Unclassified	Unclassified	Unclassified	UU	36	19b. TELEPHONE NUMBER (*Include area code*) 410-278-4762

Standard Form 298 (Rev. 8/98)
Prescribed by ANSI Std. Z39.18

Contents

List of Figures

List of Tables

INTENTIONALLY LEFT BLANK.

1. Background/Motivation for Work

Aberdeen Test Center (ATC), the U.S. Army Research Laboratory (ARL), and other Army-affiliated test organizations frequently use the Low-Frequency Foam Insulator (LOFFI) low-pass accelerometer mount for full-scale test instrumentation. An accelerometer is attached to the LOFFI mount, which is in turn attached to the system of interest, instead of mounting the accelerometer directly to the system. The rationale is that high-frequency components of the acceleration signal will otherwise saturate the accelerometer, contaminate the overall data, and thus prevent meaningful insight about low-frequency or rigid-body response modes.

The LOFFI mount (figure 1) is composed of a round aluminum baseplate that fastens to the measured system, a middle plate with three posts to which is mounted the accelerometer, and a donut-shaped top plate. Between the aluminum plates are rings of elastomeric damping material that serve to isolate the accelerometer from transmission of high-frequency vibrations.

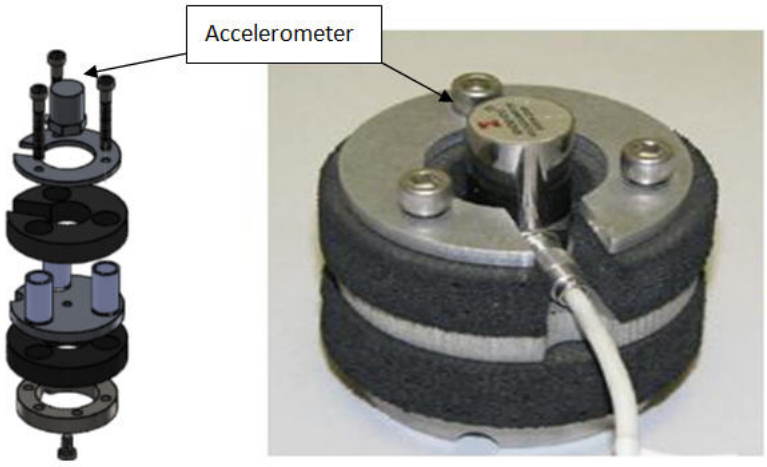

Figure 1. LOFFI accelerometer mount with aluminum and elastomeric layers.

It is known from previous testing done by ATC that the LOFFI device behaves differently than an ideal low-pass filter. As typically constructed the LOFFI has a resonance frequency of about 300 Hz, below its cutoff frequency (of about 450 Hz), and therefore, some input frequencies exist that are amplified by the resonance (figure 2). The testing done by ATC is without sufficient documentation to determine the applicability of the findings to different loading environments, including the high-acceleration pulses typically experienced in under-body blast events, so further research is required.

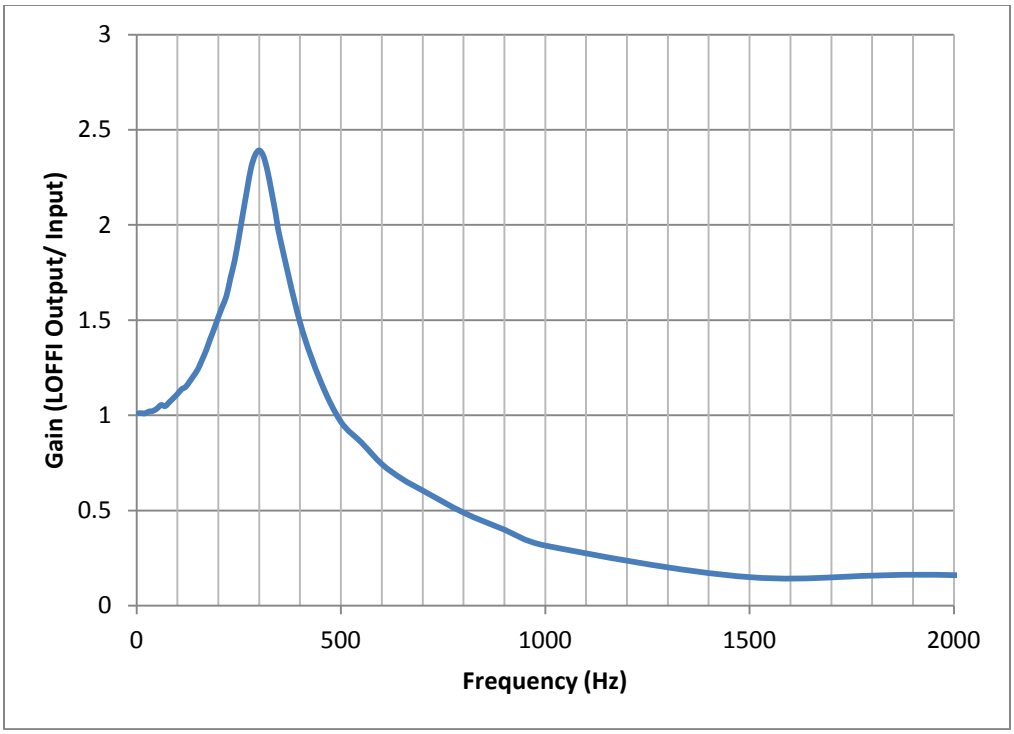

Figure 2. ATC-derived LOFFI gain function showing resonance near 300 Hz.

2. Objectives

The objectives for this project are twofold:

1. Characterize in greater detail the LOFFI mount's frequency-domain amplification ratio, referred to here as its gain function. This includes characterizing the device at a variety of acceleration magnitudes and pulse widths, including those relevant to underbody blast full-scale testing.
2. Develop a "transfer function" or set of functions to allow for the consideration or elimination of the influence of the LOFFI mount during comparisons of test results and modeling predictions. The transfer function(s) should be able to simulate the presence of a LOFFI mount when applied to modeling predictions of the system's response, or negate the presence of the mount when applied to full-scale data.*

* It should be noted that the two purposes of the transfer function may require separate solutions. The first purpose, simulating a LOFFI mount, is simply the imposition of a filter onto a data set. The negation of the mount is potentially far more complicated, or even impossible, because it involves the recovery of a high-frequency response lost or distorted by the LOFFI filtering mechanism. It may be the case that the simulation of a LOFFI mount is fairly straightforward whereas the negation of the mount requires a family of functions or cannot be satisfactorily accomplished for the general case.

3. Test Strategy and Data Collection

Testing of the LOFFI mount is divided into three phases, each performed by ARL's Weapons and Materials Research Directorate (WMRD). Phase I was completed in 2013; Phase II is scheduled for spring/summer 2014, and Phase III will be completed by the end of FY2014. Phase I consisted of 25 trials that investigated acceleration pulses with peak magnitudes between 500 and 2000 g, and pulse widths of approximately 1.5–2.0 ms. Phase II will investigate longer-duration pulses (approximately 3.5–5 ms) of lower magnitude to determine if the transfer function is still broadly applicable in that input region and if a function that parameterizes pulse width might be possible. Phase III will consist of several excursions to fill data voids of interest in the pulse magnitude-duration domain.

The test apparatus used by WMRD is a drop-tower (figure 3) with a large, rigid plate that descends onto the seismic mass from a variable height. The plate is outfitted with three accelerometers. The first is an Endevco 7270A, mounted directly to the plate, which records the "bare" or input pulse data. Two 2262-model accelerometers are each mounted to LOFFI devices; these are referred to as LOFFI 1 and LOFFI 2 in this report. The multiple LOFFI-mounted accelerometers are used to verify the measurements and give an idea of the variability of measurements between devices. Different media, such as felt, are inserted between the impacting plate and the seismic mass to control the shape and duration of the acceleration pulse that is produced on impact. These media are referred to as "programmers".

For the first nine trials of Phase I testing, a programming system of Delrin plastic (polyoxymethylene) and layers of felt were used to shape the pulses. The final 16 trials used a combination of felt and sheets of paper. (Trial 16 failed and is excluded from the remainder of this report.)

As can be seen in figures 4 and 5, the two programming systems produced qualitatively different acceleration pulses. The Delrin programmers produced wider, more rounded pulses, while the paper sheets produced a narrower, more traditional "pulse" shape with a higher peak. The fast Fourier transforms (FFTs) of the input pulses (figure 5) reflect this difference. Although the Delrin pulses have low-frequency content comparable to or higher than the paper pulses, the signal is quickly suppressed, and there are only small contributions above approximately 800 Hz. The paper programmers, meanwhile, create a broadband signal that dies away gradually, including enough high-frequency contribution that a sharper pulse can be shaped.

Figure 3. WMRD drop tower apparatus.

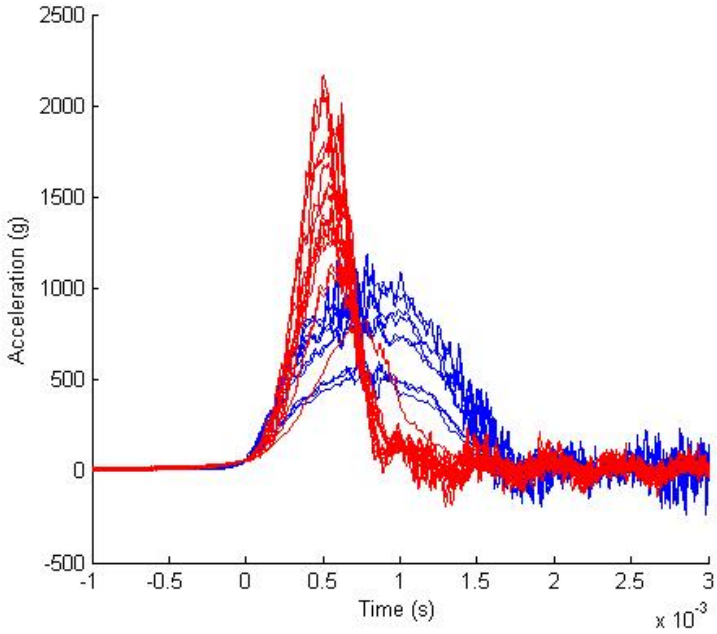

Figure 4. Aggregated acceleration time-histories for Delrin trials (blue) and paper trials (red).

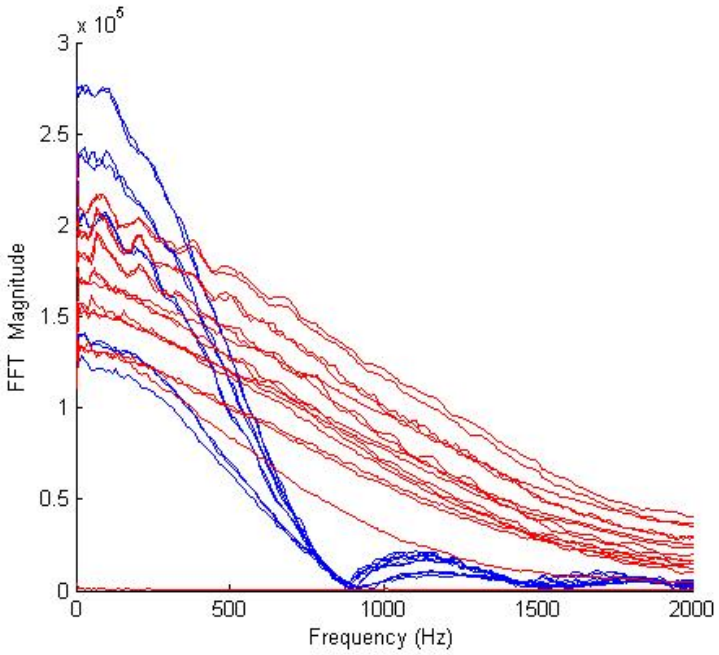

Figure 5. Aggregated frequency-domain magnitudes for Delrin trials (blue) and paper trials (red).

The different frequency contents of the input pulses potentially represent a confounding factor if the data set is analyzed as a whole. However, if the Phase I tests are first divided into sets of Delrin (9 trials) and paper (15 trials), and the analysis process is followed for each set in parallel, the differing transfer function results will reflect the sensitivity of the function to differences in input pulse characteristics. Then, after Phase III is completed, the possibility of merging the separate transfer functions into one or more "unified" transfer functions can be investigated. For this report, separate considerations of the Delrin and paper trials are pursued in the data analysis; the process is described for the paper trials in the following section, but a similar process was followed for the Delrin trials. The resulting LOFFI transfer functions are described and compared in section 5.

4. Data Analysis: Phase I

Raw data from each of the 24 trials of Phase I was saved in an individual ASCII-formatted file. The files each contained a time-domain data series from each of the three accelerometers. The data from a representative trial, Trial 19, is shown in figure 6. It can be seen that, in general, the effect of the LOFFI mount is to lessen the magnitude and lengthen the duration of the

acceleration pulse, although this is not always the case.* It is also seen that the LOFFI mounts effectively dampened high-frequency behavior—their intended purpose—and tended to perform consistently within a trial, i.e., the two mounts produced similar traces.

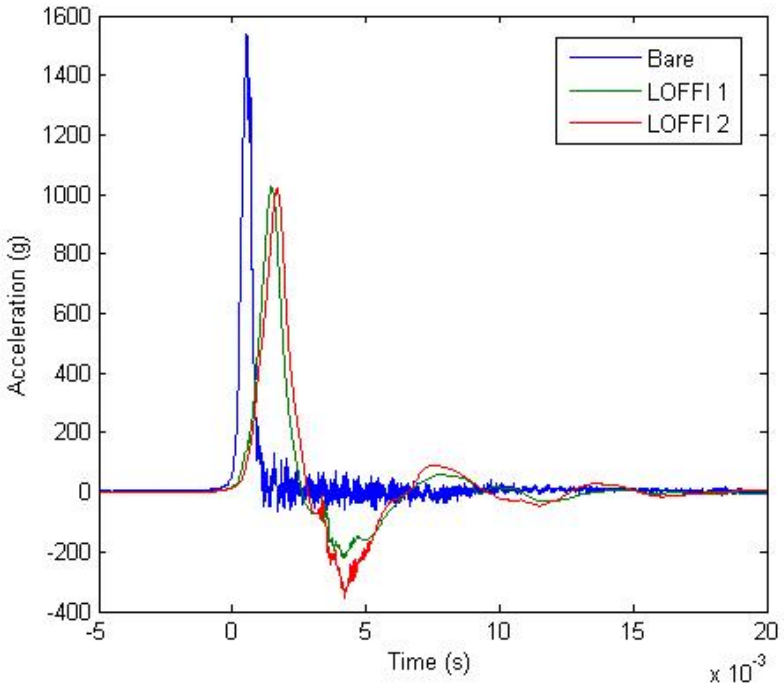

Figure 6. Time-domain data from mounted (green, red) and bare (blue) accelerometers (Trial 19).

This data was imported into MATLAB for further processing: for each accelerometer, the DC offset was calculated and removed, the peak magnitude of the main acceleration pulse was found, and the width of the pulse was calculated.† The MATLAB script then performed a FFT on each series. Zero-padding was not used. The FFT is left as double-sided, so the frequency-domain series runs from zero to twice the Nyquist frequency. The complex FFT output, F_{comp} , is then turned into magnitude data (figure 7) and phase data (figure 8) via the following transformations:

$$F_{amp}(\omega) = abs\left(F_{comp}(\omega)\right)$$

$$F_{phase}(\omega) = arctan\left(\frac{F_{imag}(\omega)}{F_{real}(\omega)}\right)$$

The MATLAB function *unwrap(angle(F))* was used in calculating the phase.

* In the first six trials, the mounts actually increased the maximum measured acceleration.

† The pulse width was calculated as the time between the points where acceleration was 20% of the maximum value divided by a factor of 0.8718. This formula assumes a haversine shape to the pulse, which was judged to be broadly accurate.

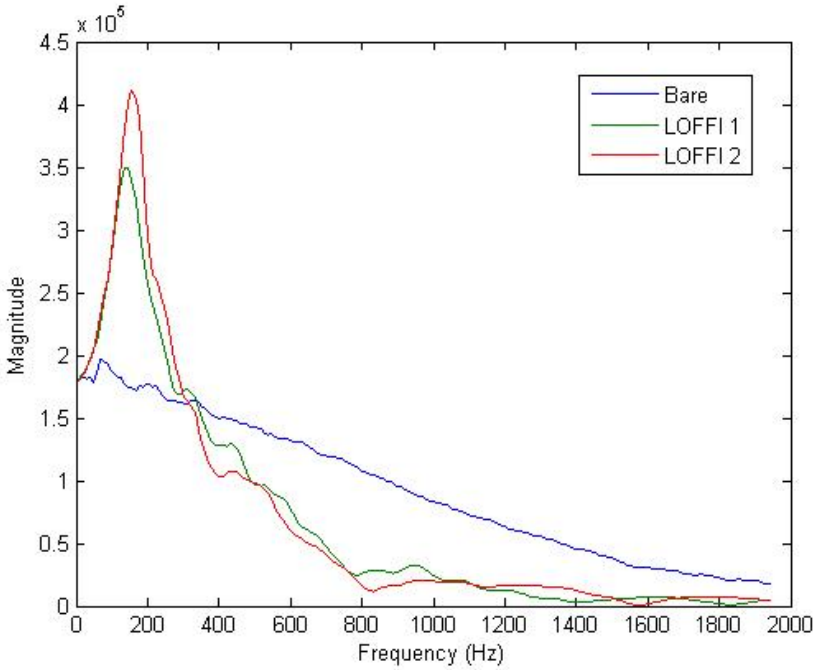

Figure 7. FFT magnitude for mounted (green, red) and bare (blue) accelerometer data (Trial 19).

Frequency-domain plots are shown here only up to 2000 Hz for clarity but the series are not truncated in the script and extend to nearly 250 kHz. Figure 7 shows the F_{amp} series for the same trial (Trial 19) shown in figure 6. As expected from the ATC gain function, it is evident in most trials that the LOFFI mount effectively dampens the broadband acceleration signal above about 400 Hz. Below this frequency, it amplifies the signal by a factor of up to about 2.5, an effect that can be seen in each trial. There also appears to be more variability in the performance between LOFFI devices in the frequency domain than is evident in the time domain.

Figure 8, meanwhile, shows only a small difference in the phase angle due to the LOFFI mount. The small jumps in the LOFFI-mounted phase series (at about 1600–1800 Hz) correspond to frequencies with near-zero magnitude, as seen in figure 7.

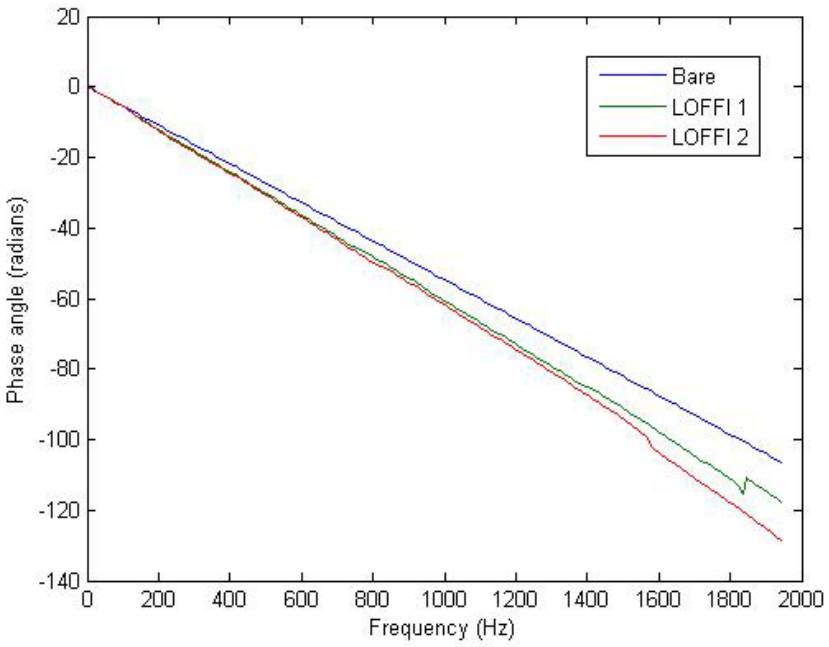

Figure 8. Phase angle for mounted (red, green) and bare (blue) accelerometer data (Trial 19).

In sum, for each of three accelerometers (bare, LOFFI 1, and LOFFI 2) in each trial, the following information was created:

- time-domain series;
- time-domain pulse magnitude and width;
- frequency series and complex FFT trace, (real) FFT magnitude, and FFT phase.

4.1 Characteristic Gain Function

There are several strategies available for producing a function that models the influence of the LOFFI device. For this report, the LOFFI's influence on the frequency-domain signal magnitude and phase are calculated separately. A simple magnitude "gain" function, $H_n(\omega)$, such as the one produced by ATC and sometimes referred to as a frequency-response function, can be realized (figure 9) by dividing each LOFFI-influenced F_{amp} series point-by-point into the corresponding F_{amp} series for the "bare" or input accelerometer.

$$H_n(\omega) = \frac{F_{amp(LOFFI)}}{F_{amp(bare)}}$$

This process produces one magnitude-based $H_n(\omega)$ for each LOFFI-mounted accelerometer and each trial. A similar set of phase "gain" functions, $P_n(\omega)$'s, are produced by subtracting the phase of the bare-mounted accelerometer from the phase of the LOFFI-mounted accelerometer.

$$P_n(\omega) = F_{phase(LOFFI)} - F_{phase(bare)}$$

The two quantities can then be combined into a complex gain function:

$$G_n(\omega) = H_n(\omega)e^{iP_n(\omega)}$$

As seen in figure 10, most trials in both programming sets produce qualitatively similar traces. The frequency-response functions show that the LOFFI mount amplifies the signal (i.e., gain is greater than 1.0) up to about 400 Hz, and reduces the signal (i.e., gain stays below 0.5) for the remainder of the spectrum. The Delrin trials produce large, erratic gains (left-hand plot, upper right corner) in frequencies above 500 Hz; because the higher-frequency content of the input pulse is so low (figure 5), gains are quite high and fluctuating. Focusing on low frequencies (right-hand plot) reveals the relative consistency of the frequency-response (magnitude gain) function across devices and programming systems below the LOFFI resonance frequency.

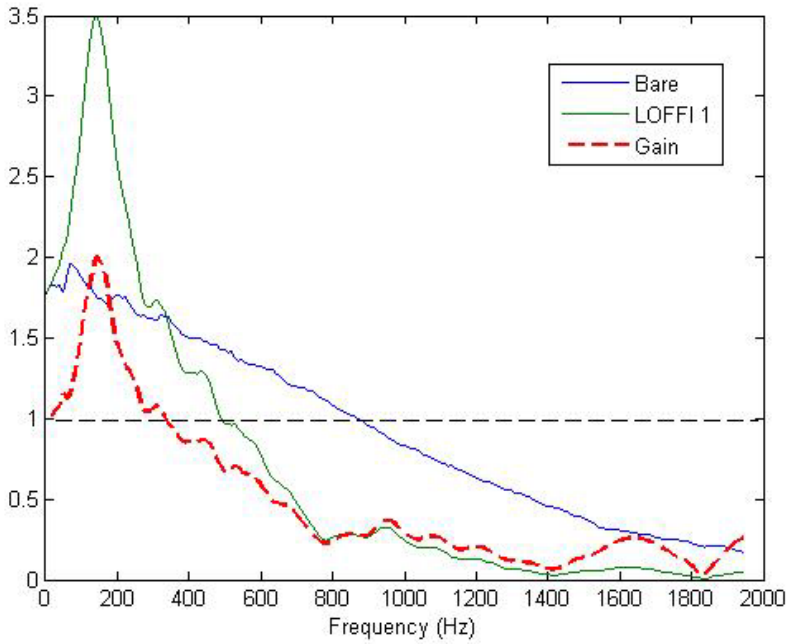

Figure 9. FFT magnitudes (as in figure 2) for mounted (green) and bare (blue) accelerometer data. Ratio of magnitudes is given as $H_{19\text{-}1}$ (red).

The median (trial-wise) H_n is identified at each frequency to produce characteristic $H(\omega)$ functions for each LOFFI device, and the two characteristic functions are averaged together to produce a single gain function that is broadly representative of a generic LOFFI device under the given conditions. This overarching $H(\omega)$ is shown in figure 11, and $P(\omega)$ is shown in figure 12.

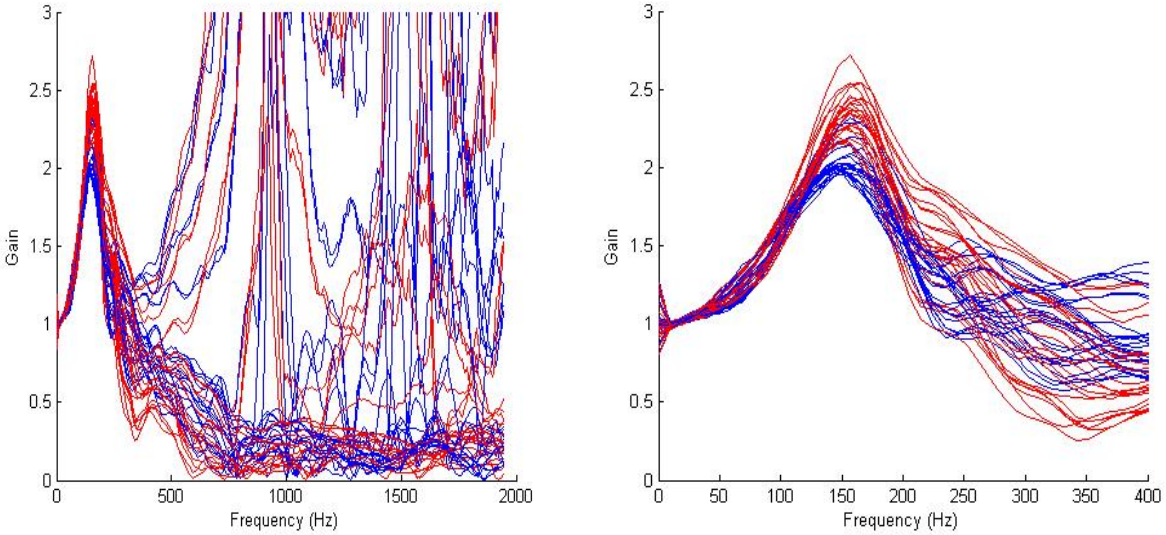

Figure 10. Aggregate views of frequency-domain gain for LOFFI 1 (blue) and LOFFI 2 (red) across all trials.

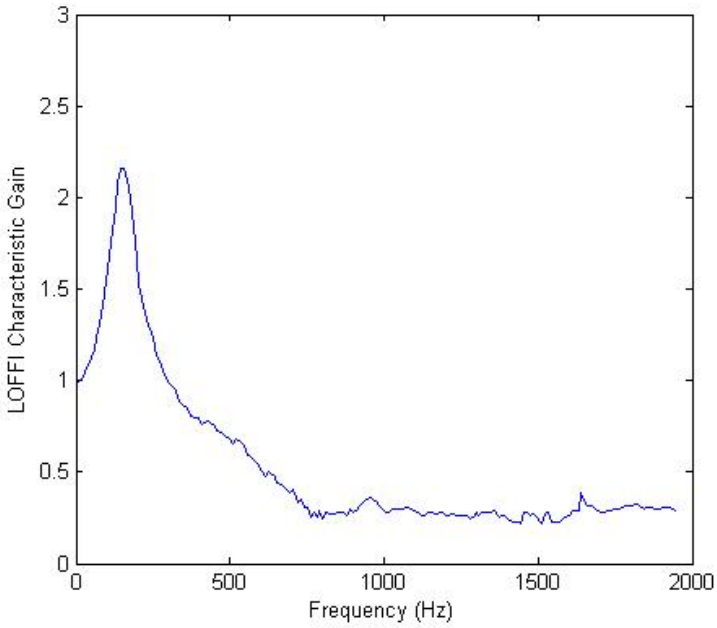

Figure 11. Frequency-domain magnitude gain of the averaged LOFFI device.

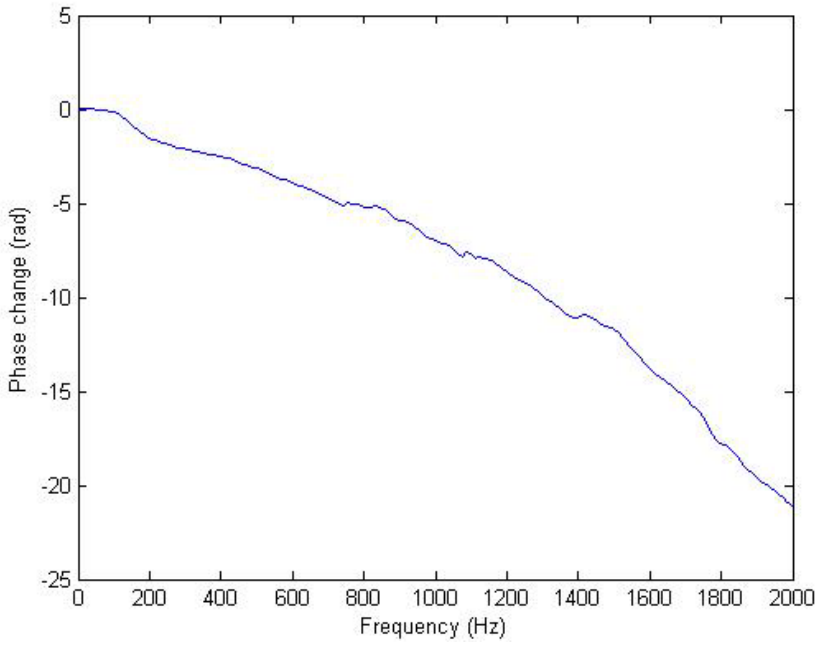

Figure 12. Frequency-domain phase gain of the averaged LOFFI device.

Once $H(\omega)$ and $P(\omega)$ are available, there are two ways to check the gain functions, corresponding to the two purposes of the functions laid out in the second objective. Either the gain function can be superimposed on top of "bare" data to reproduce LOFFI-influenced data (the input-to-LOFFI transformation), or the LOFFI-influenced data can be divided by the gain function to reproduce bare data (LOFFI-to-input).

4.2 LOFFI-to-Input Transformation (LOFFI Negation)

The more complicated application, and thus perhaps the more difficult to check, is negation of the LOFFI influence. To check the functions this way, every $F_{amp(LOFFI)}$ series can be divided by $H(\omega)$, and every $F_{phase(LOFFI)}$ series subtracted by $P(\omega)$, respectively. The results, denoted as F'_{amp} and F'_{phase}, should approximate the $F_{amp(bare)}$ and $F_{phase(bare)}$ series from unmounted accelerometers for the same trial.

$$F'_{amp}(\omega) = \frac{F_{amp(LOFFI)}}{H(\omega)} \approx F_{amp(bare)}$$

$$F'_{phase}(\omega) = F_{phase(LOFFI)} - P(\omega) \approx F_{phase(bare)}$$

This was done for the same representative trial (Trial 19) in figures 13 and 14. F'_{amp} and F'_{phase} are referred to as the "adjusted" LOFFI series in the figures.

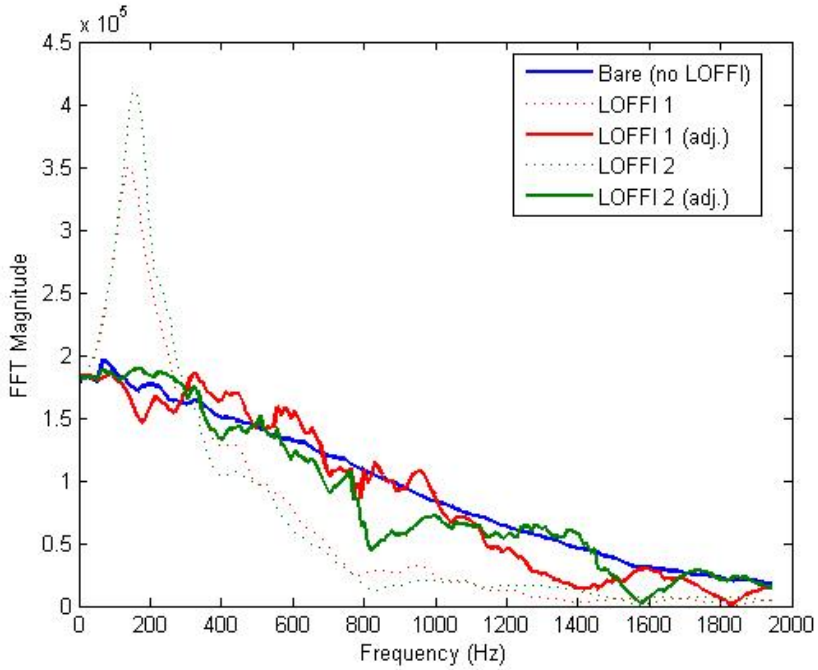

Figure 13. Adjusted (solid) and unadjusted (dashed) FFT magnitudes (Trial 19).

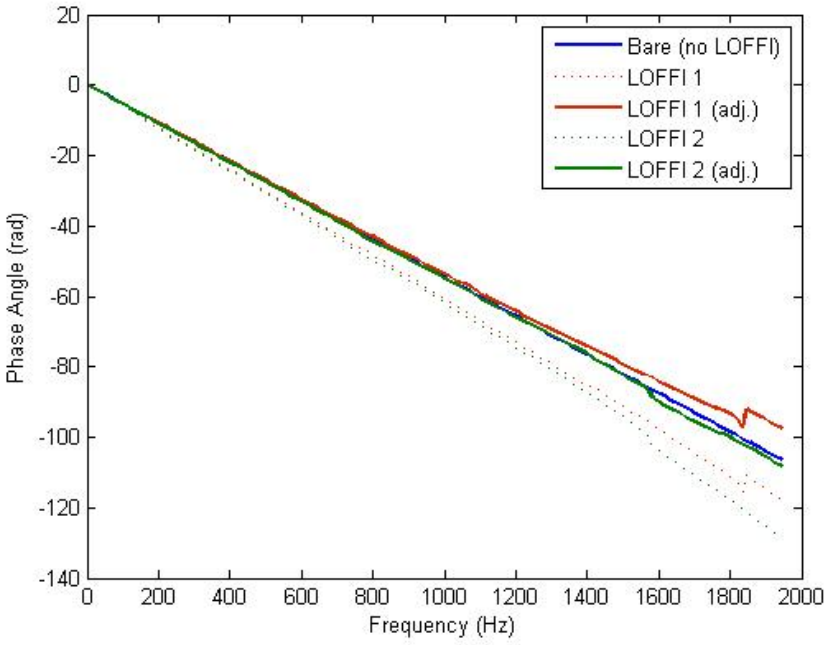

Figure 14. Adjusted (solid) and unadjusted (dashed) FFT phase angles (Trial 19).

The preceding figures show a significant improvement in the adherence of the LOFFI-mounted data to the input data values in the frequency domain. The large amplification below 400 Hz has disappeared, and the dampening effect above 400 Hz is largely gone as well. Meanwhile, phase angle tracks much more closely to the non-LOFFI input data.

If the reconstructed *F'* magnitude and phase series are correct, the time-domain pulse should resemble the pulse recorded by the bare accelerometer. To see how the reconstructed pulse appears, the F'_{amp} and F'_{phase} series were converted to the complex form via the transformation

$$F'_{comp}(\omega) = F'_{amp} * e^{iF'_{phase}}$$

and then an inverse FFT was performed on the resulting complex data series to return to the time domain. (In practice, the MATLAB *ifft()* command would return a complex series, so the absolute value was used.) This reconstructed pulse is shown in figure 15 compared to both the unadjusted LOFFI data and non-LOFFI input data from figure 4 to see if the influence of the LOFFI mount had been eliminated.

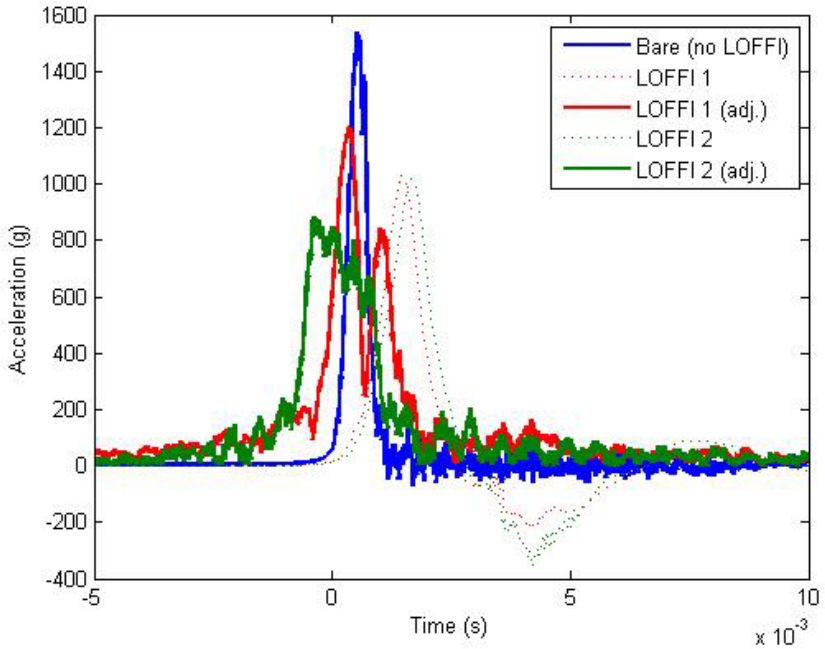

Figure 15. Adjusted (solid) and unadjusted (dashed) time-domain pulse data (Trial 19).

As can be seen, simply applying $H(\omega)$ and $P(\omega)$ does not yield a significant improvement in the time-domain pulses. The peaks of the main acceleration pulse are still well below the input peak and the pulse appears even wider than in the unadjusted data. This problem is evident for each trial; typically, reconstructed pulses are 50%–70% the peak magnitude of the baseline pulse. However, the timing of the peaks appear to be improved enough that the reconstructed pulse coincides with the bare pulse, as opposed to lagging behind as observed with the raw LOFFI-mounted pulses.

An evident source of error is the “jaggedness” of the adjusted FFT magnitude series as compared to the baseline non-LOFFI series. Figure 13 shows relatively small perturbations around a quasi-linear trend, but in some other trials there is a great deal of oscillation. For example, figure 16 shows the adjusted FFT magnitudes for Trial 13 where wide deviations from the trendline are apparent. Additionally, regions of the adjusted FFT spectrum deviate considerably from the expected pulse profile due to the average gain function being insufficiently representative of the data for that trial at those frequencies. These errors lead to reconstructed time-domain pulses that do not resemble the input data.

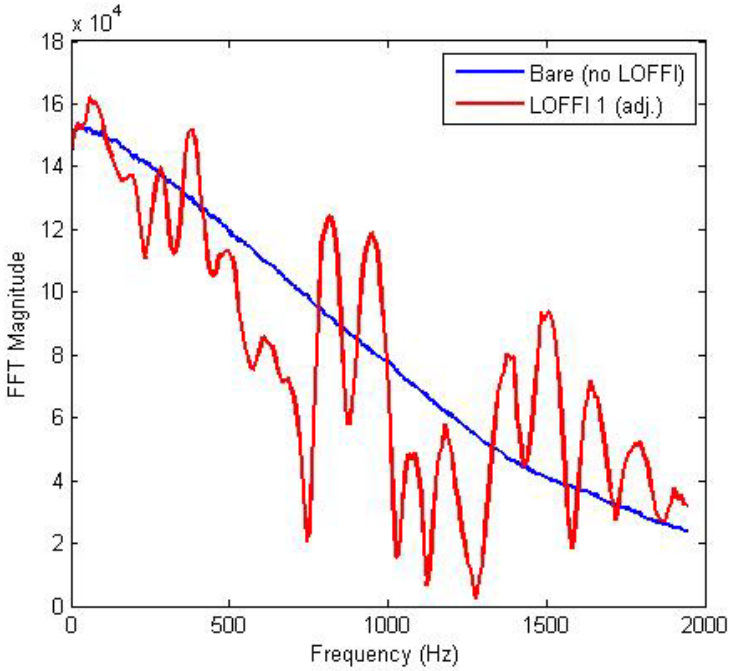

Figure 16. Adjusted LOFFI FFT spectrum and input data (Trial 13).

To correct for these deviations, a curvefit was applied in the frequency domain to F'_{amp}, thereby smoothing the most jagged oscillations by replacing the data with a trendline. Deciding on the type of fit (and the bounding parameter values) involved ensuring that the resulting curve conformed to the general “character” of the input (unmounted) data without overfitting the function (i.e., forcing it to match).

For the LOFFI-to-input transformation, a simple two-part piecewise fit was chosen; a weighted third-degree polynomial fit* for the low-frequency portion of the spectrum where the FFT magnitude is above a threshold value, and a very low value after that which served to zero out the FFT at higher frequencies.† Parameters (refer to footnote *) were chosen to enforce a general shape (for example, the coefficient of the cubic term had to be positive) but were otherwise relaxed in order to avoid overfitting. Lower-frequency data was prioritized by the curvefit weighting function so that the fit matched the regions of experimental interest (and greatest magnitude) most carefully. Figures 17 and 18 show the calculated fit, the underlying F'_{amp} data, and the non-LOFFI data ($F_{amp(bare)}$) for both the representative trial (Trial 19) and the more poorly behaved trial (Trial 13) from figure 16.

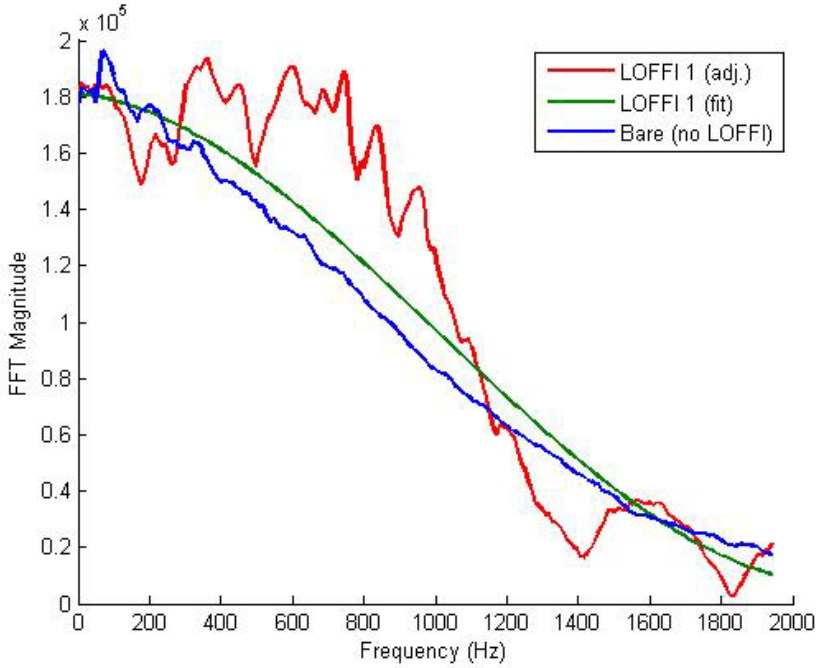

Figure 17. Curve fit for adjusted LOFFI magnitude (Trial 19).

*Weighting: 1/frequency. Upper bounds on polynomials: 0.05, 0.5, 0.0, Inf. Lower bounds: 0, -10, -Inf, -Inf. Mid-range frequencies above the LOFFI cut-off (between approximately 400 Hz and approximately 900 Hz) were excluded so that fit would focus on connecting the high-confidence values at low frequencies and at frequencies above approximately 2000 Hz.

†Because this effectively created a single-sided FFT spectrum, the inverse FFT was doubled.

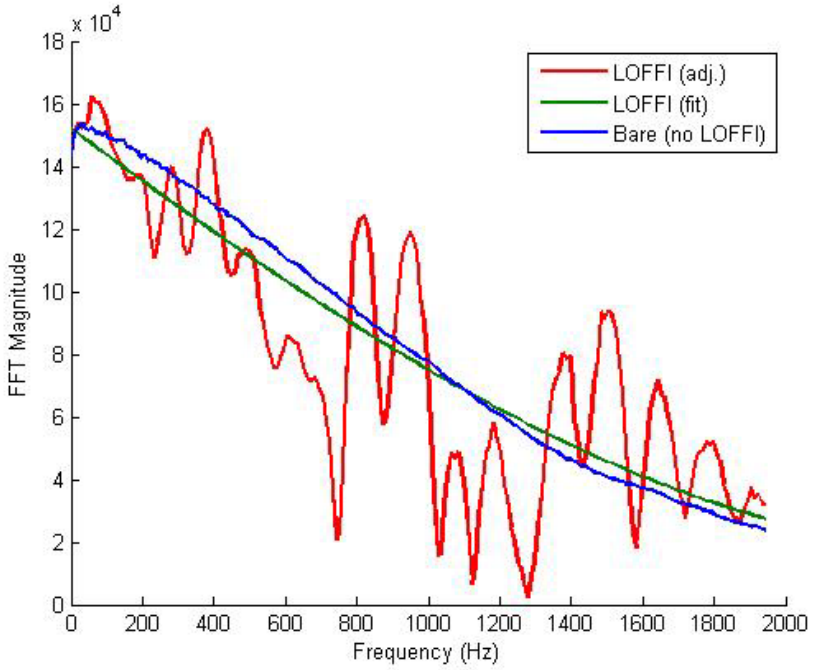

Figure 18. Curve fit for adjusted LOFFI magnitude (Trial 13).

In general, the curve-fit adjusted LOFFI series conforms much more closely (and smoothly) to the input data than the discrete series does. This is reflected in the time-domain pulse reconstruction (figure 19).

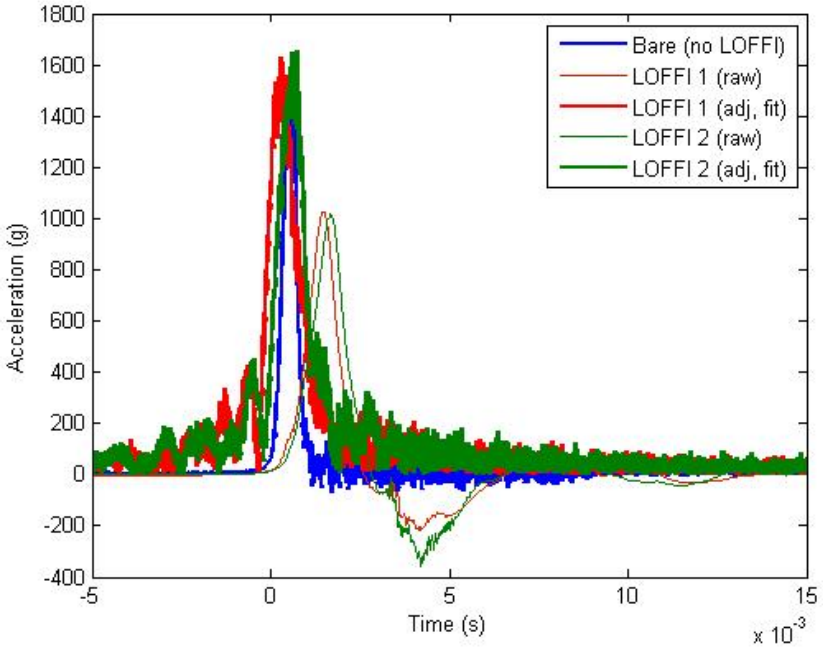

Figure 19. Adjusted and curve-fit (thick) and unadjusted (thin) time-domain pulse data (Trial 19).

It is clear that the curve-fit series is a much more suitable approximation for the input pulse than the discrete series (shown in figure 15) or the unadjusted "raw" series. Trial 19 is particularly well-behaved, but even poorly behaved trials such as Trial 13 show improved resemblance between the curve-fit LOFFI series and the bare input series (figure 20).

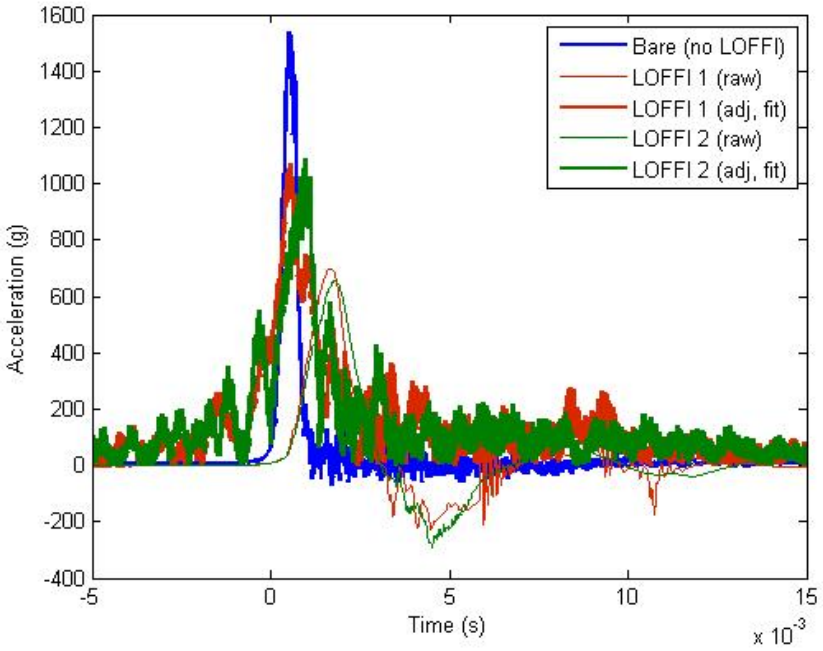

Figure 20. Adjusted and curve-fit (thick) and unadjusted (thin) time-domain pulse data (Trial 13).

It can be seen in figure 20, and later in the results section, that the loss of high-frequency response data during the physical LOFFI filtering cannot always be accurately compensated for by this transformation process. The reason is that substantially different input pulses, when filtered through the low-pass LOFFI mount, can produce very similar output if the original difference is due to high-frequency contributions. The similarity of the output means that certain information is completely lost. Since this effect of the LOFFI mount is not a straightforward 1:1 process, the reverse LOFFI-to-input transformation will often produce inaccurate pulses, and the hope is by averaging the gain functions of many trials to produce a function that works "well enough" for a given future event. This suggests that the ability to accurately negate the LOFFI mount will decrease with shorter input pulses that contain greater high-frequency content. Therefore it may be necessary, going forward, to define an "operating envelope" of input pulse characteristics in which LOFFI usage is recommended.

4.3 Input-to-LOFFI Transformation (LOFFI Simulation)

More consistent success is possible with the simpler input-to-LOFFI (simulation) transformation because the transformation uses "complete" input data that has not had the high-frequency content already mechanically removed. In this case, the adjusted series is arrived at by superimposing the gain functions on top of the frequency-domain input pulse:

$$F'_{amp}(\omega) = F_{amp(bare)} * H(\omega)$$

$$F'_{phase}(\omega) = F_{phase(bare)} + P(\omega)$$

$$F'_{comp}(\omega) = F'_{amp} * e^{iF'_{phase}}$$

Note that for the simulation transformation, *F'*, the adjusted frequency-domain series, represents the **addition** of a LOFFI instead of its subtraction as in the previous section. The final quantity (F'_{comp}) then represents the simulation of a LOFFI device on a bare accelerometer, either real or modeled. This F'_{comp} series is already sufficiently smooth to produce a reasonable inverse FFT output without additional curve-fitting. The final data processing simply finds the frequency at which F'_{comp} first drops below a small number (example 2000) and replaces the remainder of the series with that number. As in the LOFFI-to-input transformation, this produces an effectively one-sided FFT series, so the output of the inverse FFT is doubled. The result is the completion of the input-to-LOFFI transformation.

As figure 21 shows, agreement between the adjusted input series and the LOFFI-mounted data is (for the representative case) very good, and this is true in general as well. To allow negative values in the trace, the real portion of the complex output was used instead of the absolute value. This did not significantly affect the timing of the peak acceleration or its magnitude, but it did allow the simulated LOFFI pulse to follow the true LOFFI measurements much more closely after the peak.

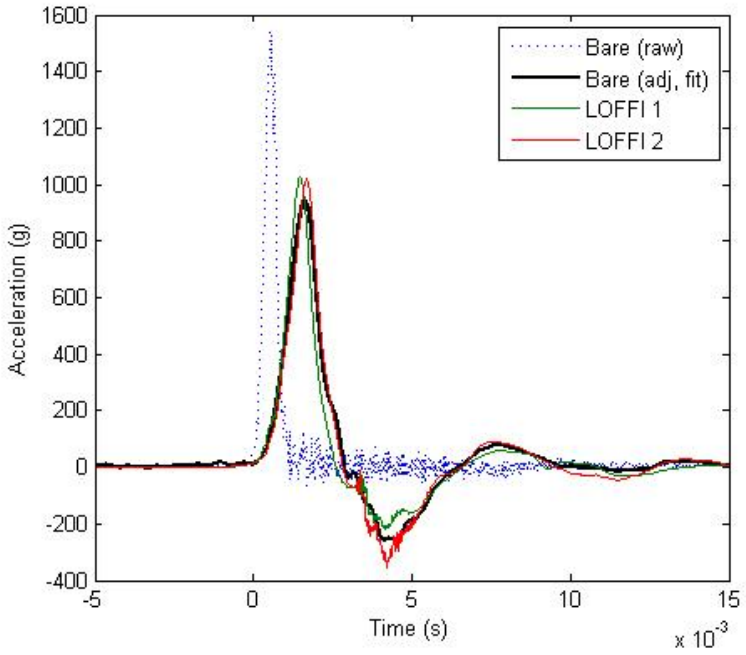

Figure 21. Adjusted and curve-fit (thick) and unadjusted (thin) time-domain pulse data (Trial 19).

5. Overall Results: Phase I

As stated previously, the data analysis process was executed separately for the Delrin programming trials and the paper programming trials because the nature of the underlying input pulse appeared to be sufficiently different (figure 5). Once more diverse sets of trials have been performed in Phases II and III, the goal will be to merge the separate gain curves into a parameterized family of curves, i.e., create a generalized gain curve that is a function of some aspect of the input data. For now it is sufficient to discuss the two individual sets (Delrin and paper) of input data separately.

Table 1 highlights the effectiveness of the LOFFI negation transformation, which is seen as less accurate than the simulation transformation. In the table, α is defined as the mean ratio of the LOFFI-mounted accelerometer's peak magnitude to the bare accelerometer's peak magnitude. (Thus, 1.0 signifies a perfectly transparent mount.) The σ is the standard deviation of those ratios, or a measure of how much spread is present in the ratio between different trials. Subscripts "0" and "T" represent "without" and "with" the LOFFI-to-input transformation, respectively.

Table 1. Comparison of raw data to LOFFI-to-input transformed data for both programming systems.

Delrin	α_0	σ_0	α_T	σ_T
LOFFI 1	1.46	0.43	1.07	0.18
LOFFI 2	1.49	0.57	1.09	0.18
Paper	α_0	σ_0	α_T	σ_T
LOFFI 1	0.61	0.08	0.90	0.16
LOFFI 2	0.58	0.09	0.95	0.16

Without the corrective transformation, both LOFFIs show a large overmeasurement with the Delrin programmer, and a large undermeasurement with the paper programmer. Additionally, the Delrin measurements are quite scattered (large σ). With the negation transformation, the reconstructed-pulse data converge on the bare accelerometer data significantly (α approaches 1.0) under both programming systems. The only penalty is a slight gain in dispersal with paper programming.

Both the discussion of the characteristic gain function for each programming medium, and the efficacy of the related simulation and negation transformations on a case-by-case basis, are provided in the following sections.

5.1 Characteristic Gain Function

The characteristic gain curves associated with the Phase I trials are shown in figure 22. It shows that, as predicted by figure 10, the Delrin trials produced a characteristic gain very similar to that associated with the paper trials for frequencies under about 400 Hz. After that point, the erratic nature of the gain functions of individual trials causes the median gain to remain relatively elevated. At irregular intervals (approximately 900 and 1450 Hz) the gain function is especially high; frequencies corresponding to the near-zeroes shown in figure 5. It is theorized that the relatively low absolute signal levels at high frequencies make the erratic gain function less concerning for analysis purposes, so no effort was made to correct the function or otherwise smooth the high-frequency peaks.

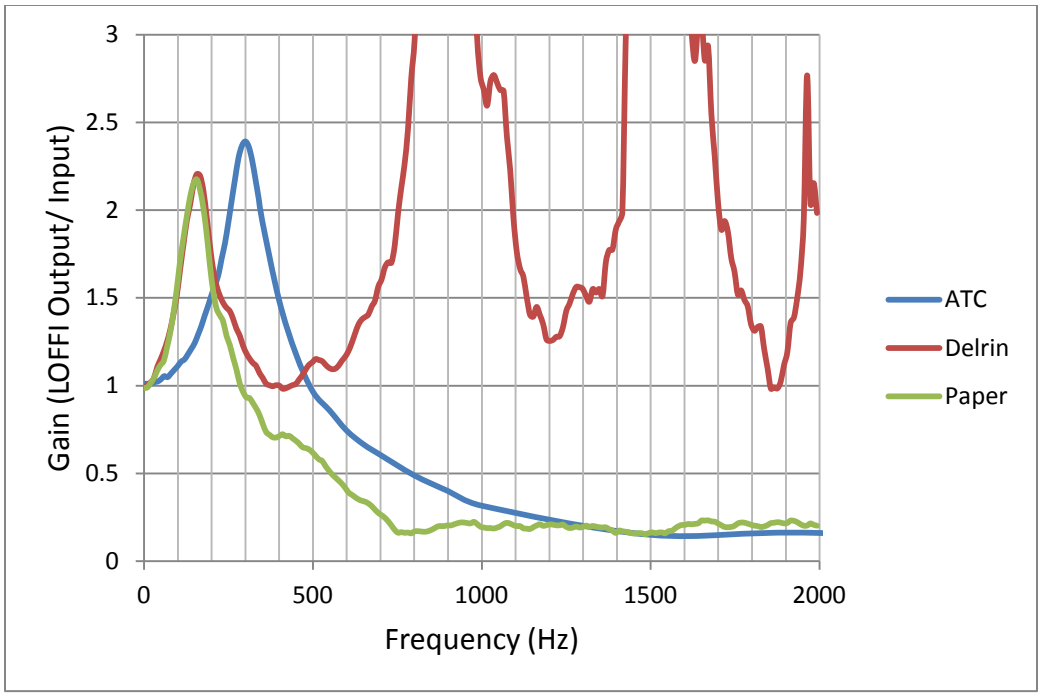

Figure 22. LOFFI characteristic gain.

The characteristic gain associated with the paper trials is more "well-behaved". The paper-programmer gain function does not have peaks associated with low-input magnitudes until well past the 2000-Hz range depicted in these plots. Qualitatively, it is quite similar to the ATC gain function, although the particulars differ somewhat. It exhibits a resonance frequency lower (175 Hz) than ATC's findings of 300 Hz. It also reaches a minimal value at as low as 700 Hz, as opposed to ATC's findings of over 1500 Hz.

5.2 Delrin: Input-to-LOFFI Transformation (LOFFI Simulation)

Figure 23 displays the peak acceleration magnitude measured by each trial's two LOFFI devices plotted against the peak magnitude read by the bare input accelerometer. The hollow circles represent a peak LOFFI measurement (y-axis) and the peak bare measurement (x-axis) from the same trial. The filled circles represent the same LOFFI peaks, but with the bare measurements adjusted by the gain function to simulate a LOFFI device. Thus, the filled data points will be translated left or right of the corresponding hollow data points. (Ideally, the filled points will lie along the dashed "input = output" line on each figure.) The dashed line represents equal values for "real" and "simulated" LOFFI peak measurements; ideally, the filled points are translated until they lie on or near the line.

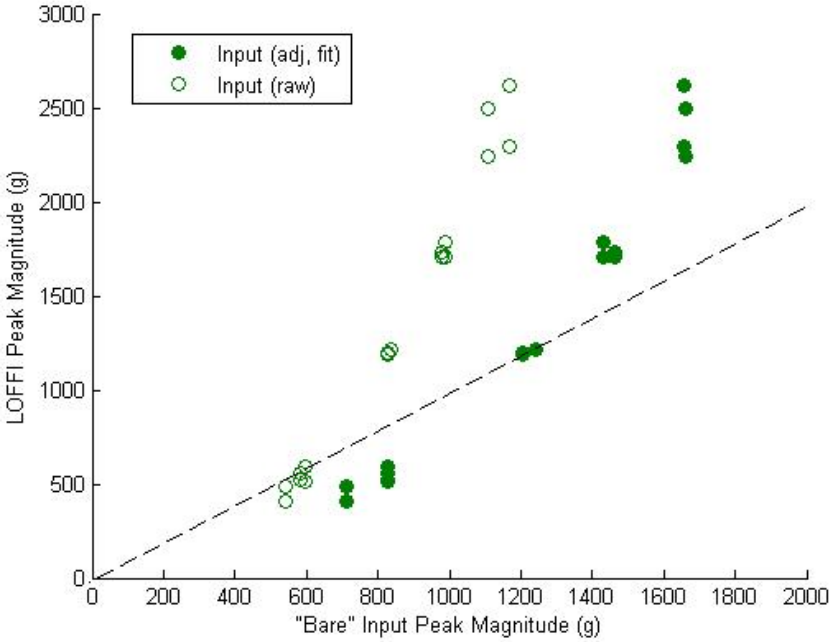

Figure 23. Comparison of LOFFI peak acceleration to reconstructed peak acceleration (Delrin).

Figure 23 shows significant improvement in correlation between the input accelerometer and the LOFFI-mounted accelerometers due to the transformation process. In most cases the input peak magnitude moves much closer to parity with the LOFFI-mounted peaks. Additionally, a near-linear placement of the adjusted data points is observed. This suggests that the extent to which the transformation process over-predicts or under-predicts the LOFFI-mounted acceleration might be a simple function of peak acceleration magnitude, and that additional corrections could be possible to further increase the accuracy of the transformation.

5.3 Delrin: LOFFI-to-Input Transformation (LOFFI Negation)

The more complicated reverse transformation involves removing (or at least accounting for) the influence of the LOFFI mount from the filtered data it produces. In figure 24, unadjusted LOFFI data is shown as hollow circles, and adjusted (and curve-fit) data is represented with filled circles. Again, the dashed trendline represents a perfect match between input and output peak magnitudes, so the filled circles will ideally be translated up or down from the hollow circles toward the dashed line.

Figure 24 shows that for Delrin experiments, the negation transformation reduces the over-measurement of the LOFFI-mounted accelerometers significantly and reduces the spread of the data as well. For the Delrin programmers, the significant over-measurement by the LOFFI-mounted accelerometers almost completely disappears once the transformation is applied. Meanwhile, for the trials where good accuracy already existed, it is not significantly compromised.

Table 1 provides a quantification of the effects of the LOFFI negation transformation process for both programmers.

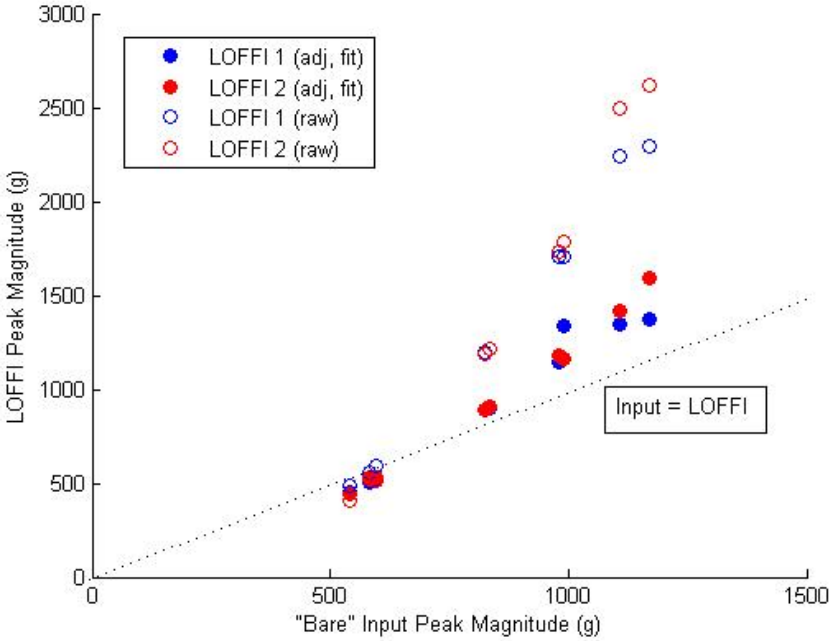

Figure 24. Comparison of input peak acceleration to reconstructed input peak acceleration (Delrin).

5.4 Paper: Input-to-LOFFI Transformation (LOFFI Simulation)

Figure 25 shows for paper-programmer trials that, as with the Delrin programmer trials, the transformation process significantly reduces the difference between bare-mounted acceleration data and LOFFI-mounted data. In this case, however, it is a strong undermeasurement of the peak acceleration that is corrected. This is true over a wide range of input peak accelerations, between 800 and nearly 2200 g, or most of the working range of the accelerometers.

Again, the adjusted data appears to be linearly laid out (with higher-magnitude peaks above the parity line and lower-magnitude peaks at or below it) suggesting that further data correction might be possible. A correction factor was not applied at this time because of the lack of a clear rationale for choosing one besides empirical fit. However, one will be suggested after the final phase of data collection if trends in the data suggest that a simple expression is sufficient.

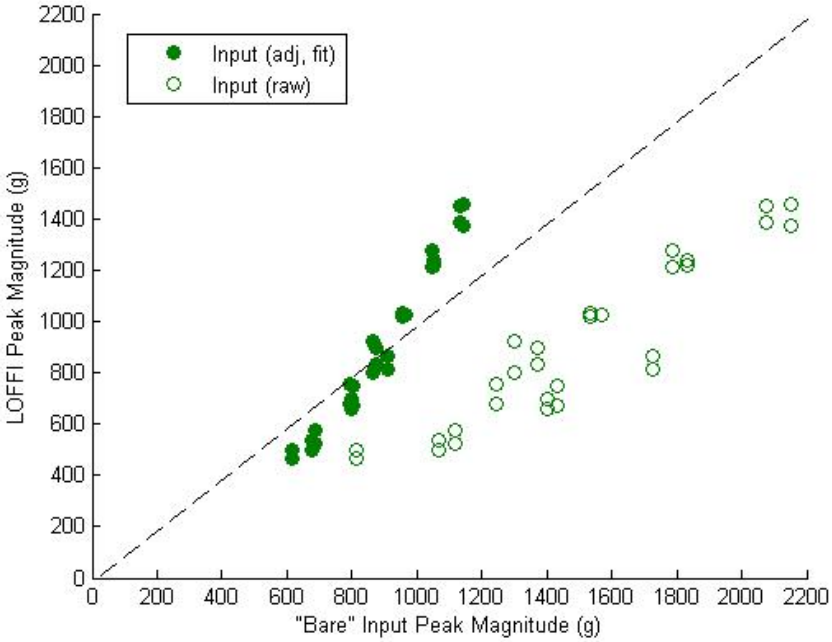

Figure 25. Comparison of LOFFI peak acceleration to reconstructed peak acceleration (paper).

5.5 Paper: LOFFI-to-Input Transformation (LOFFI Negation)

The peak magnitude comparison in figure 26 again shows significant increase in the similarity of pulse magnitudes after the LOFFI-to-input transformation was applied. This is especially true at higher input magnitudes, where the LOFFI-mounted accelerometers improved from greatly under-reporting the peak acceleration to very slightly over-reporting.

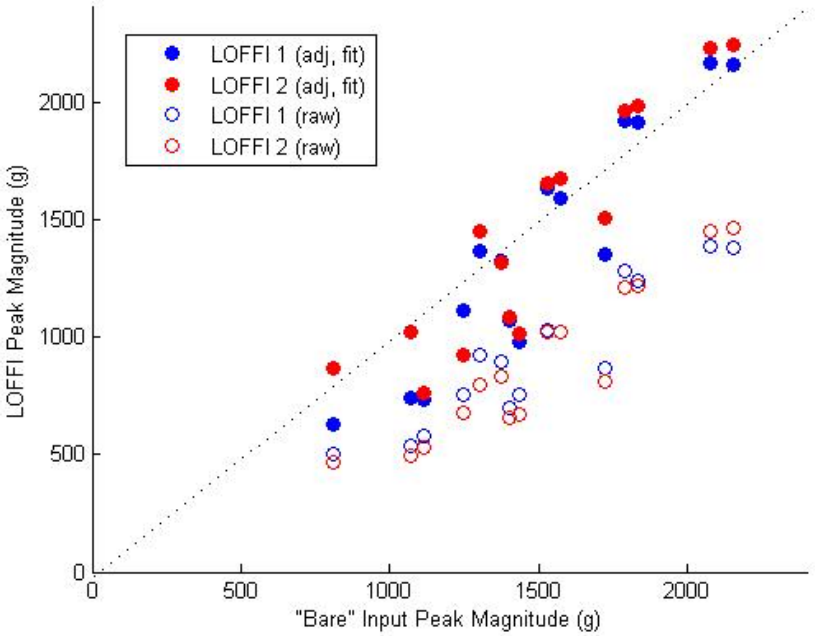

Figure 26. Comparison of input peak acceleration to reconstructed peak acceleration (paper).

6. Discussion/Path Forward

After the completion of Phase I, several observations can be made that reflect on the results presented in the previous section. These observations will guide the next phases of experimental work as scheduled for FY2014.

1. At least in certain conditions, the general accuracy of the ATC frequency-response function is confirmed, although a more precise function is now available. A transformation process is now available to greatly improve the "transparency" of the LOFFI mount, or reduce its effect on acceleration measurements.

2. Further work is needed to combine the Delrin- and paper-programmer gain functions into a single "unifying" function that has at least one variable parameter. It is not yet clear what quantity that parameter should represent, although one good candidate is the slope of the frequency-domain drop-off (figure 5) in the mid-frequency region. Experimental work in future phases will hopefully provide additional pulse shapes for comparison.

3. Further work is needed to produce gain functions for additional pulse widths and magnitude levels in order to extend the usefulness of the transformation process. This should be addressed at least to some degree in Phases II and III.

4. Time permitting, other sources of nonlinear behavior by the LOFFI mount should be investigated. Examples include the age/usage of the foam, the type of material comprising the foam layer, and the torque/compression of the foam during installation.

5. Finally, some comparison of input data series to full-scale data and examples of finite-element modeling must be done to ensure that “real-world” data resembles the test data, at least qualitatively. Otherwise Phases II and III should be amended to reflect these likely applications of the transformation process.

1 (PDF) DEFENSE TECHNICAL INFORMATION CTR DTIC OCA

2 (PDF) DIRECTOR US ARMY RESEARCH LAB RDRL CIO LL IMAL HRA MAIL & RECORDS MGMT

1 (PDF) GOVT PRINTG OFC A MALHOTRA

1 (HC) DIR US ARMY EVALUATION CTR HQ TEAE SV P A THOMPSON 2202 ABERDEEN BLVD 2ND FL APG MD 21005-5001

8 (3 HC 5 PDF) DIR USARL
RDRL SL
J BEILFUSS (HC)
P TANENBAUM (HC)
RDRL SLB S
M PERRY
RDRL SLE
R FLORES
RDRL SLB D
A DRYSDALE (HC)
RDRL WMP F
R S SORENSEN
J E PRITCHETT

INTENTIONALLY LEFT BLANK.